Realization of the Dicke Model Using Cavity-Assisted Raman Transitions

Markus P. Baden,[1] Kyle J. Arnold,[1] Arne L. Grimsmo,[2] Scott Parkins,[3] and Murray D. Barrett[1,4,*]
[1]Centre for Quantum Technologies, 3 Science Drive 2, Singapore 117543
[2]Department of Physics, The Norwegian University of Science and Technology, N-7491 Trondheim, Norway
[3]Department of Physics, University of Auckland, Private Bag 92019, Auckland, New Zealand
[4]Department of Physics, National University of Singapore, 3 Science Drive 2, Singapore 117543
(Received 2 April 2014; published 10 July 2014)

We realize an open version of the Dicke model by coupling two hyperfine ground states using two cavity-assisted Raman transitions. The interaction due to only one of the couplings is described by the Tavis-Cummings model and we observe a normal mode splitting in the transmission around the dispersively shifted cavity. With both couplings present the dynamics are described by the Dicke model and we measure the onset of superradiant scattering into the cavity above a critical coupling strength.

DOI: 10.1103/PhysRevLett.113.020408 PACS numbers: 05.30.Rt, 42.50.Nn, 42.50.Pq

Ultracold atoms coupled to a high-finesse optical cavity have become a versatile tool for studying many-body physics in dissipative-driven systems [1]. For example, a theoretical proposal [2] suggested the use of cavity-assisted Raman transitions to realize an open version of the Dicke model [3] in order to study the properties of the associated superradiant phase transition [4,5]. Following this idea, the process of self-organization [6–8] of a Bose-Einstein condensate coupled to a high-finesse cavity has been mapped to the Dicke model [9,10] and the corresponding phase transition has been observed [9]. Together with subsequent work [11–14] this experiment has in turn led to interesting theoretical studies into the properties of the Dicke model [15–19] and the dynamics of a wider class of nonequilibrium models [20–22]. However, mapping to the process of self-organization constrains the range of accessible parameter regimes. In contrast, by implementing the original proposal [2] all parameters of the Dicke model are independently tunable. In addition, the original idea has been extended in ways which allow the study of more complex many-body systems such as the Lipkin-Meshkov-Glick model [23,24] and spin glasses [25,26], as well as the effects of modulating the parameters of the Dicke model [27–29]. Studies of the nonequilibrium Dicke models as well as their extensions will profit from the flexibility inherent in the original proposal.

In this letter, we realize an effective Dicke model using two cavity-assisted Raman transitions. Coupling due to one Raman transition alone creates a situation described by the Tavis-Cummings model [30] and we measure the normal mode splitting present in the transmission spectrum of the cavity, which allows us to characterize the effective atom-cavity coupling strength. With the second Raman coupling present, the dynamics are governed by the Dicke model and we observe the onset of superradiant scattering into the cavity above a critical coupling.

Our experimental scheme follows closely the original proposal [2], with a slightly altered level scheme, which was recently considered for the case of a single atom [31]. The details of our experimental setup have been described previously [32]. We trap N rubidium 87 atoms inside the mode volume of a high finesse optical cavity and couple the $|F=1, m_F=1\rangle \equiv |0\rangle$ and $|F=2, m_F=2\rangle \equiv |1\rangle$ hyperfine ground states via two cavity-assisted Raman transitions as illustrated in Fig. 1. In order to have well separated Zeeman states, we apply a magnetic field of approximately -5.7 Gauss. At this field the $|0\rangle$ and $|1\rangle$ states are separated by $\omega_1 = \omega_{\mathrm{hf}} - 3\omega_Z$, where $\omega_{\mathrm{hf}} = 2\pi \times 6.8347$ GHz is the hyperfine splitting of the ground state and $\omega_Z \approx 2\pi \times 4.0$ MHz is the linear Zeeman shift [33]. The cavity has a

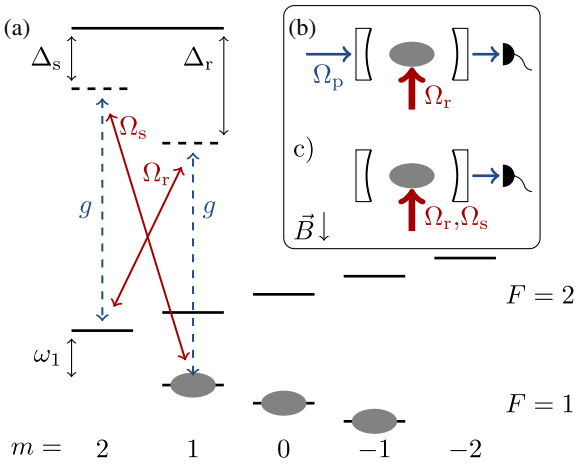

FIG. 1 (color online). Schematic representation of the experiment. (a) We trap N rubidium 87 atoms, indicated by the filled ellipses, in a equal mixture of hyperfine states inside a high finesse optical cavity. Two laser beams with Rabi frequencies Ω_r and Ω_s, indicated by solid arrows, are far detuned from the excited state but near resonant with the cavity-assisted Raman transition, indicated by dashed arrows. (b) With only one beam present, we probe the cavity transmission and observe a normal mode splitting. (c) With both beams present, we observe emission into the cavity above the critical coupling.

finesse of 110 000 near 780 nm and 150 000 near 1560 nm. The high finesse at 1560 nm allows us to stabilize the length of the cavity, and create a deep intracavity optical lattice, using light at 1556 nm. The resulting lattice used to trap the atoms during the experiment has a waist of 70 μm and is actively stabilized to a trap depth of 230 μK. Near 780 nm the interaction of the atoms with the cavity is described in terms of the cavity QED parameters $(g,\kappa,\gamma) = 2\pi \times (1.1, 0.07, 3.0)$ MHz, where $2g$ is the single photon Rabi frequency for the $|F = 2, m_F = 2\rangle$ to $|F' = 3, m_{F'} = 3\rangle$ cycling transition, and κ and γ are the half-width-half-maximum linewidths of the cavity and atomic transition respectively. Due to birefringence, the two linear polarization modes of the cavity are split by 0.29 MHz. We align the magnetic field to one of the polarizations, so that the two modes couple to π and $\perp = 1/\sqrt{2}(\sigma^+ + \sigma^-)$ transitions respectively, and that the one coupling to π transitions has a higher resonance frequency. Two laser beams with Rabi frequencies Ω_r and Ω_s are copropagating perpendicular to the cavity optical axis and are linearly polarized along the cavity axis, so that they couple to $\perp' = 1/\sqrt{2}(\sigma^+ - \sigma^-)$ transitions. Both beams have a waist of 110(10) μm at the position of the atoms.

Our experiments are performed in the dispersive regime, where the cavity resonance frequency, ω_c, is far detuned from the atomic resonance frequency, ω_a, by $\Delta_c = \omega_c - \omega_a = -2\pi \times 127$ GHz. The frequencies of the laser beams are given by

$$\omega_r = \omega_c + \eta - \omega_{hf} - \zeta \tag{1}$$

and

$$\omega_s = \omega_c + \eta + \omega_{hf} + \zeta, \tag{2}$$

respectively, where both η and ζ are small frequency offsets on the order of several megahertz. In this regime, there is a small differential Stark shift,

$$\omega_{dS} \approx \frac{1}{6}\left(\frac{\Omega_r^2}{\Delta_r} + \frac{\Omega_s^2}{\Delta_r - \omega_1} - \left(\frac{\Omega_s^2}{\Delta_s} + \frac{\Omega_r^2}{\Delta_r - \omega_1}\right)\right), \tag{3}$$

between the $|1\rangle$ and the $|0\rangle$ states that must be taken into account for the experiments presented here. In Eq. (3) and throughout this work we follow the convention that Rabi frequencies are calculated from the dipole element for the $|F = 2, m_F = 2\rangle$ to $|F' = 3, m_{F'} = 3\rangle$ cycling transition [33].

As all detunings, Δ_c, $\Delta_r = (\omega_r + \omega_1) - \omega_a$ and $\Delta_s = \omega_s - \omega_a$, are much larger then the hyperfine splittings of the excited state manifold [33], the Raman rate for transitions involving $\perp$ and $\perp'$ is negligible, as these connect states with different nuclear spin components. Only two Raman transitions, involving π and $\perp'$, are near to Raman resonance. The first takes the atom from the $|0\rangle$ to the $|1\rangle$ state via absorption of a photon from the laser beam labeled by s and emission into the cavity (and its reverse), while the second takes the atom from the $|0\rangle$ to the $|1\rangle$ state via absorption of a photon from the cavity and emission into the laser beam labeled by r (and its reverse). We note in particular that the Raman transition taking the atom from the $|0\rangle$ to the $|F = 2, m_F = 0\rangle$ state is detuned by $2\omega_Z \approx 2\pi \times 8.0$ MHz from Raman resonance. Taking into account the relevant transition strengths, the cavity couplings for the two nearly resonant Raman processes are identical.

After performing the adiabatic elimination of the excited states [2] and neglecting any off resonant transitions [31], the system, in a suitable rotating frame defined in the Supplemental Material [34], is described by the master equation ($\hbar = 1$)

$$\dot{\rho} = -i[H, \rho] + \mathcal{L}\rho, \tag{4}$$

with

$$H = \omega a^\dagger a + \omega_0 J_z + \frac{\delta}{N_\lambda} a^\dagger a J_z + \frac{\lambda_r}{\sqrt{N_\lambda}}(a J_+ + a^\dagger J_-) + \frac{\lambda_s}{\sqrt{N_\lambda}}(a^\dagger J_+ + a J_-), \tag{5}$$

and

$$\mathcal{L}\rho = \kappa(2a\rho a^\dagger - a^\dagger a\rho - \rho a^\dagger a). \tag{6}$$

Here a ($a^\dagger$) is the annihilation (creation) operator for the cavity mode,

$$J_+ = \sum_{j=1}^{N_\lambda} |1\rangle_j\langle 0|, \qquad J_- = \sum_{j=1}^{N_\lambda} |0\rangle_j\langle 1|, \tag{7}$$

and

$$J_z = \frac{1}{2}\sum_{j=1}^{N_\lambda} (|1\rangle_j\langle 1| - |0\rangle_j\langle 0|) \tag{8}$$

are the collective atomic operators satisfying the commutation relations $[J_+, J_-] = 2J_z$ and $[J_\pm, J_z] = \mp J_\pm$,

$$\omega = \alpha\frac{1}{3}N\left(\frac{g^2}{\Delta_s} + \frac{g^2}{\Delta_r}\right) - \alpha\frac{1}{3}N_{\bar{\lambda}}\left(\frac{g^2}{\Delta_s} - \frac{g^2}{\Delta_r}\right) - \eta, \tag{9}$$

$$\omega_0 = \omega_{dS} - (\omega_{hf} + \zeta - \omega_1), \tag{10}$$

$$\delta = \alpha\frac{2}{3}N_\lambda\left(\frac{g^2}{\Delta_s} - \frac{g^2}{\Delta_r}\right), \tag{11}$$

$$\lambda_r = \beta\frac{\sqrt{3}}{12}\frac{\sqrt{N_\lambda}g\Omega_r}{\Delta_r}, \qquad \lambda_s = \beta\frac{\sqrt{3}}{12}\frac{\sqrt{N_\lambda}g\Omega_s}{\Delta_s}, \tag{12}$$

where $N_\lambda \approx N/3$ is the number of atoms in the coupled states $|1\rangle$ and $|0\rangle$, $N_{\bar{\lambda}} = N - N_\lambda$, and $\alpha \approx 0.66$ and

$\beta \approx 0.78$ are averaging factors taking into account the spatial averaging of the cavity coupling due to thermal motion. The averaging is described in more detail in the Supplemental Material [34], together with a derivation of Eq. (5) and an account of how we generate the necessary Raman couplings.

To realize the Dicke model we set $\Omega_r = \Omega_s$. For our detuning from the excited state the difference between the two Raman couplings is small, $(\lambda_s - \lambda_r)/(\lambda_s + \lambda_r) \approx 0.028$, so we set $\lambda_r \approx \lambda_s = \lambda$ and arrive at

$$H = \omega a^\dagger a + \omega_0 J_z + \frac{\delta}{N_\lambda} a^\dagger a J_z + \frac{\lambda}{\sqrt{N_\lambda}}(a + a^\dagger)(J_+ + J_-). \tag{13}$$

Similarly, we can describe the situation of a single Raman coupling by setting $\Omega_s = 0$ and $\Omega_r > 0$. Assuming the atoms remain in the $F = 1$ hyperfine ground state manifold, we combine ω and the constant term proportional to δ and arrive at the Tavis-Cummings model [30],

$$H = (\omega_d - \eta) a^\dagger a + \omega_0 J_z + \frac{\lambda_r}{\sqrt{N_\lambda}}(a J_+ + a^\dagger J_-), \tag{14}$$

where

$$\omega_d = \alpha \frac{2}{3} N \frac{g^2}{\Delta_r} \tag{15}$$

is the dispersive shift of the cavity resonance due to N atoms in the lower hyperfine ground state manifold.

We start our experiments by forming a magneto-optical trap 15 mm above the cavity. At the end of the magneto-optical trapping phase we pump the atoms into the $F = 1$ hyperfine manifold and load up to 5×10^6 atoms into a single-beam optical dipole trap at 1064 nm. The beam forming the dipole trap is moved down by 15 mm over one second by a translation stage. Upon arrival in the cavity, we adiabatically lower the power in the 1064 nm trap and transfer the atoms into the intracavity optical lattice. By varying the number of atoms in the magneto-optical trap, we control the number of atoms delivered to the intracavity trap, up to a maximum of 2×10^5. After loading, we nondestructively determine the atom number by measuring the dispersive shift ω_d, with an accuracy of approximately 5 kHz. To do this, we sweep the frequency of a weak probe beam across the dispersively shifted cavity. The Rabi frequency of the probe beam, Ω_p, has been adjusted to yield an average intracavity photon number on resonance of $\langle n \rangle \approx 40$, to allow for sufficient signal to noise. After measuring the dispersive shift, we either turn on the Tavis-Cummings coupling and measure the transmission through the cavity, or we ramp up the strength of the Dicke coupling and observe the onset of superradiance by monitoring the scattering into the cavity. Both experiments are described in more detail below. At the end of the experimental sequence we remeasure the dispersive shift to determine atom loss during the experiment and we repeat the cycle. During the experiment, we detect the output light of the cavity which is coupled into a single mode fiber and directed onto a single photon counting module (SPCM).

First we characterize our system by measuring the normal mode splitting present in the Tavis-Cummings model. To do so, we set $\eta = 0$, $\zeta \neq 0$ and pulse Ω_r on for 1 ms, with a power of 18(1) mW in the coupling beam. Simultaneously, we pulse the probe beam on for 1 ms and sweep its detuning relative to the empty cavity, $\Delta_p = \omega_p - \omega_c$, from $\Delta_p = -2\pi \times 1.4$ MHz to $\Delta_p = -2\pi \times 0.1$ MHz. In the presence of the coupling beam, the system shows an avoided crossing in the transmission spectrum around $\omega = \omega_0$ and the size of the splitting is given by $2\lambda_r$. Experimentally, we vary the atom number for a fixed ζ, which changes both ω and λ_r, and leads to the transmission spectra shown in Fig. 2. From the normal mode splitting we infer $\omega_1 + \omega_{dS} - \omega_{hf} = -2\pi \times 12.02(32)$ MHz and $\lambda_r = 2\pi \times 0.173(15)$ MHz at a dispersive shift of $\omega_d = -2\pi \times 0.50(1)$ MHz.

A central feature of the Dicke model is a phase transition into a superradiant state once the coupling reaches a critical value, which for ω_0, $\omega > 0$ is given by [21]

$$\lambda_c = \frac{1}{2}\sqrt{\frac{\omega_0}{\omega - \delta/2}(\kappa^2 + (\omega - \delta/2)^2)}. \tag{16}$$

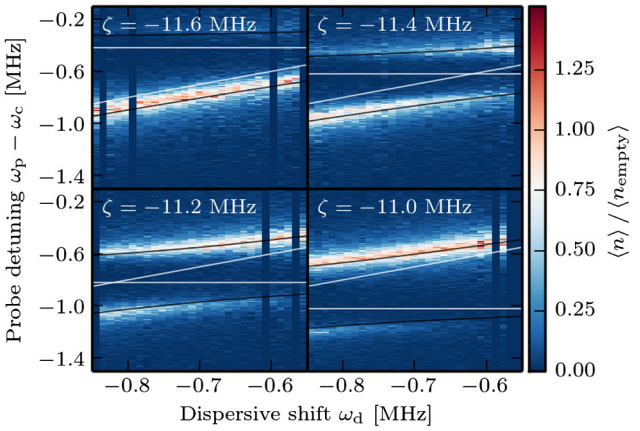

FIG. 2 (color online). Normal-mode splitting in the Tavis-Cummings model. For a single coupling beam present, the cavity transmission spectrum shows a normal mode splitting around the dispersively shifted resonance. We vary the atom number for a fixed λ_r and ζ, record the cavity transmission $\langle n \rangle$ normalized by the empty cavity transmission $\langle n_{empty} \rangle$ and average traces corresponding to dispersive shifts in 10 kHz bins. Gray lines indicate the bare energies $\omega_0 = -2\pi \times 12.02$ MHz $- \zeta$ and $\omega = \omega_d$. Black lines indicate the eigenenergies of the coupled system for a coupling of $\lambda_r = 2\pi \times 0.17$ MHz for a dispersive shift of $\omega_d = -2\pi \times 0.5$ MHz. Transmission in excess of 1 is due to shot noise exceeding the amplitude of the Lorentzian used to fit the empty cavity transmission.

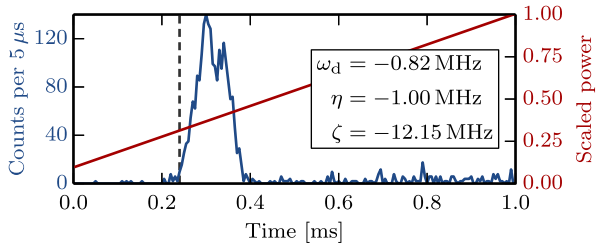

FIG. 3 (color online). Single threshold measurement. We ramp the total power in both Raman coupling beams over 1 ms (diagonal red line) and observe the output of the cavity (blue curve). The critical coupling is inferred from when the output of the cavity reaches 7.8 counts/(5 μs), indicated by the dashed line, which corresponds to an intracavity photon number of 10 and is 10 times higher than the background counts.

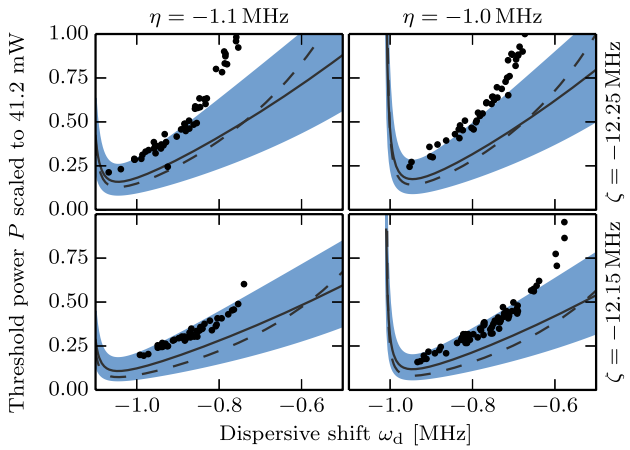

FIG. 4 (color online). Superradiant phase transition in the Dicke model. Above a critical coupling, the system undergoes a phase transition into a superradiant state. Black dots show the observed threshold values. The solid gray line shows the theoretical predictions for a calculated differential stark shift of $\omega_{\mathrm{dS}} = -2\pi \times 0.157$ MHz and $\omega_1 = -2\pi \times 11.94$ MHz and $\lambda = 2\pi \times 0.173$ MHz at a dispersive shift of $\omega_{\mathrm{d}} = -2\pi \times 0.5$ MHz, as obtained from the normal-mode splitting measurement. The blue shaded area shows the upper and lower bounds inferred from the same measurement where the coupling for the lower bound is increased by a factor of 1.2 and the one for the upper decreased by a factor of 0.89 to account for the varying amount of spontaneous emission. The dashed line is derived from the normal-mode splitting measurement assuming $\omega_{\mathrm{dS}} = 0$ to illustrate the effect of the varying differential stark shift.

We note that the critical coupling depends on the power in the coupling beams because ω_0 varies with the differential stark shift ω_{dS}. To observe the phase transition for a particular $\eta \neq 0$ and $\zeta \neq 0$, we start with both beams at a low power such that the coupling is well below the critical value and then linearly increase the total power, P, over 1 ms from 3.6(2) mW to 36(2) mW. We identify the critical coupling by a rapid increase in the cavity output as shown in Fig. 3. Experimentally, we again vary the atom number, which changes both ω and λ, resulting in the observed threshold powers shown in Fig. 4.

The observed thresholds are higher than expected from simple theory, Eq. (16). There are four possible mechanisms for this: thermal motion of the atoms, atom loss during the experiment, spontaneous emission, and delays in the onset of superradiance. Thermal motion has already been taken into account by the averaging factor β and does not have a strong dependence on temperature. Atom loss is less then 10% and is thus unlikely to be a significant contributing factor. Spontaneous emission, however, is significant and we estimate a scattering rate of 0.55 ms^{-1} for a power of 18 mW in each Raman beam. We also note that, for a fixed atom number N_λ and cavity coupling g, the Raman coupling λ fixes the amount of population in the excited state since $P_e \propto \Omega_{\mathrm{r}}^2/\Delta_{\mathrm{r}}^2 \propto \lambda_{\mathrm{r}}^2/(N_\lambda g^2)$, independent of the chosen detuning from the excited state. Spontaneous emission will tend to depump the atoms from the collective spin state and thus decrease the effective coupling strength. This effect is also present in the Tavis-Cummings model, which we use to infer the effective coupling. Thus, if the power in each of the Raman beams for the threshold measurement was the same as for the splitting measurement, we could expect the same coupling. However, the total power at the beginning (end) of the Dicke experiment is 0.2 (2.0) times the power in Fig. 2. A corresponding decrease (increase) in spontaneous emission leads to a larger (smaller) coupling than what we would have expected based on the ratio of powers. Repeating the measurement of Fig. 2 at 0.2 (2.0) times the power we measure a splitting that deviates by 1.2 (0.89) from that expectation. The blue shaded region in Fig. 4 takes the corresponding uncertainty in estimating the coupling from the splitting measurement into account. There is a remaining discrepancy in the observed thresholds. We believe this is due to delays in the onset of superradiance. When ramping the power in finite time, there is a delay between crossing the threshold and observing light from the cavity [9]. This leads to a systematic overestimation of the threshold. To account for this would require extending previous theoretical frameworks [21] to include spontaneous emission and is an interesting avenue for future research.

In summary, we have demonstrated the ability to use cavity-assisted Raman transitions in order to create tunable atom-photon interactions. We have both studied the Tavis-Cummings and the Dicke model in this setup and shown that the effective cavity and spin frequencies are easily varied. Being able to both weakly probe the system and to dynamically change the couplings put our setup in an ideal situation to investigate the dynamics and steady state properties of the Dicke model and its generalizations. Furthermore the scheme presented in this work could be easily extended to include additional couplings, more atomic states or additional cavity modes [35], for example by making use of the second birefringent mode present in

our setup. In this work we have explored the regime where the effective atom-photon coupling exceeds the cavity decay rate and residual spontaneous emission can not be neglected. Future studies could explore a regime where the critical coupling is much reduced in order to avoid this problem, or add incoherent repumping to explore the regime of steady-state superradiance [36].

We would like to thank Ferdinand Brennecke for the many helpful discussion about the related experiments done in the Esslinger group at ETH Zurich. We acknowledge the support of this work by the National Research Foundation and the Ministry of Education of Singapore, as well as by A-STAR under Project No. SERC 052 123 0088.

*phybmd@nus.edu.sg

[1] H. Ritsch, P. Domokos, F. Brennecke, and T. Esslinger, Rev. Mod. Phys. **85**, 553 (2013).
[2] F. Dimer, B. Estienne, A. S. Parkins, and H. J. Carmichael, Phys. Rev. A **75**, 013804 (2007).
[3] R. H. Dicke, Phys. Rev. **93**, 99 (1954).
[4] K. Hepp and E. H. Lieb, Phys. Rev. A **8**, 2517 (1973).
[5] K. Hepp and E. H. Lieb, Ann. Phys. (N.Y.) **76**, 360 (1973).
[6] P. Domokos and H. Ritsch, Phys. Rev. Lett. **89**, 253003 (2002).
[7] A. T. Black, H. W. Chan, and V. Vuletić, Phys. Rev. Lett. **91**, 203001 (2003).
[8] S. Slama, S. Bux, G. Krenz, C. Zimmermann, and P. W. Courteille, Phys. Rev. Lett. **98**, 053603 (2007).
[9] K. Baumann, C. Guerlin, F. Brennecke, and T. Esslinger, Nature (London) **464**, 1301 (2010).
[10] D. Nagy, G. Kónya, G. Szirmai, and P. Domokos, Phys. Rev. Lett. **104**, 130401 (2010).
[11] K. Baumann, R. Mottl, F. Brennecke, and T. Esslinger, Phys. Rev. Lett. **107**, 140402 (2011).
[12] R. Mottl, F. Brennecke, K. Baumann, R. Landig, T. Donner, and T. Esslinger, Science **336**, 1570 (2012).
[13] F. Brennecke, R. Mottl, K. Baumann, R. Landig, T. Donner, and T. Esslinger, Proc. Natl. Acad. Sci. U.S.A. **110**, 11763 (2013).
[14] D. Schmidt, H. Tomczyk, S. Slama, and C. Zimmermann, Phys. Rev. Lett. **112**, 115302 (2014).
[15] D. Nagy, G. Szirmai, and P. Domokos, Phys. Rev. A **84**, 043637 (2011).
[16] B. Öztop, M. Bordyuh, Ö. E. Müstecaplıoğlu, and H. E. Türeci, New J. Phys. **14**, 085011 (2012).
[17] W. Kopylov, C. Emary, and T. Brandes, Phys. Rev. A **87**, 043840 (2013).
[18] M. Kulkarni, B. Öztop, and H. E. Türeci, Phys. Rev. Lett. **111**, 220408 (2013).
[19] Y. Zhang, J. Lian, J.-Q. Liang, G. Chen, C. Zhang, and S. Jia, Phys. Rev. A **87**, 013616 (2013).
[20] J. Keeling, M. J. Bhaseen, and B. D. Simons, Phys. Rev. Lett. **105**, 043001 (2010).
[21] M. J. Bhaseen, J. Mayoh, B. D. Simons, and J. Keeling, Phys. Rev. A **85**, 013817 (2012).
[22] A. L. Grimsmo and A. S. Parkins, J. Phys. B **46**, 224012 (2013).
[23] S. Morrison and A. S. Parkins, Phys. Rev. Lett. **100**, 040403 (2008).
[24] S. Morrison and A. S. Parkins, Phys. Rev. A **77**, 043810 (2008).
[25] P. Strack and S. Sachdev, Phys. Rev. Lett. **107**, 277202 (2011).
[26] S. Gopalakrishnan, B. L. Lev, and P. M. Goldbart, Phys. Rev. Lett. **107**, 277201 (2011).
[27] V. M. Bastidas, C. Emary, B. Regler, and T. Brandes, Phys. Rev. Lett. **108**, 043003 (2012).
[28] G. Vacanti, S. Pugnetti, N. Didier, M. Paternostro, G. M. Palma, R. Fazio, and V. Vedral, Phys. Rev. Lett. **108**, 093603 (2012).
[29] L. Yu, J. Fan, S. Zhu, G. Chen, S. Jia, and F. Nori, Phys. Rev. A **89**, 023838 (2014).
[30] M. Tavis and F. W. Cummings, Phys. Rev. **170**, 379 (1968).
[31] A. L. Grimsmo and S. Parkins, Phys. Rev. A **87**, 033814 (2013).
[32] K. J. Arnold, M. P. Baden, and M. D. Barrett, Phys. Rev. Lett. **109**, 153002 (2012).
[33] D. Steck, Rubidium 87 d line data, http://steck.us/alkalidata (revision 2.1.4, December 23, 2010).
[34] See Supplemental Material at http://link.aps.org/supplemental/10.1103/PhysRevLett.113.020408 for a detailed derivation of the effective models and a description of the Raman laser setup.
[35] J. Fan, Z. Yang, Y. Zhang, J. Ma, G. Chen, and S. Jia, Phys. Rev. A **89**, 023812 (2014).
[36] J. G. Bohnet, Z. Chen, J. M. Weiner, D. Meiser, M. J. Holland, and J. K. Thompson, Nature (London) **484**, 78 (2012).